Unraveling gelation kinetics, arrested dynamics and relaxation phenomena in filamentous colloids by photon correlation imaging (Supplementary Information)

Mattia Usuelli,[a,‡] Vincenzo Ruzzi,[b,‡] Stefano Buzzaccaro,[b] Gustav Nyström,[a,c] Roberto Piazza,[*,b] and Raffaele Mezzenga[*,a,d]

1 AFM analysis of the formed amyloid fibrils

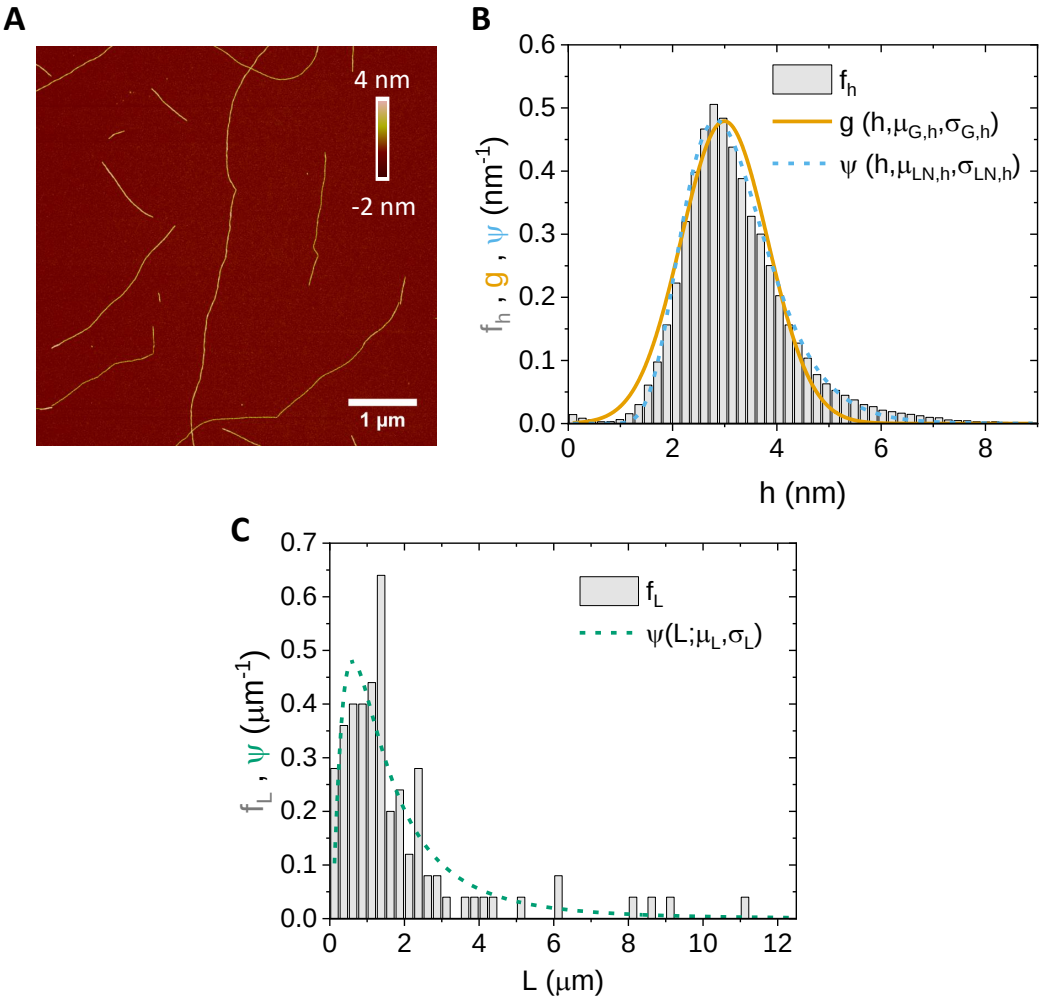

Fig. S1 AFM (Atomic Force Microscopy) analysis of the formed amyloid fibrils, which were tracked using the open-source software FiberApp[1]. (**A**) Cropped version of the original AFM image, where the semi-flexible fibrils are clearly visible. (**B**) Probability density function of the height of the fibrils, which can be approximated to their diameter. The two fittings are respectively Gaussian (g, ochre solid line) and log-normal (ψ, light blue dashed line): both of them have a most probable value around 3 nm. (**C**) Probability density function of the length of the fibrils. The log-normal fit (ψ, green dashed line), despite not being accurate due to the limited number of fibrils present in the examined AFM images, shows a significant fraction of the population having a length larger than 1 μm.

‡ These authors contributed equally to this work
[a] *ETH Zürich, Department of Health Sciences and Technology, Schmelzbergstrasse 9, 8092 Zürich, Switzerland. E-mail: raffaele.mezzenga@hest.ethz.ch*
[b] *Department of Chemistry, Materials Science, and Chemical Engineering (CMIC), Politecnico di Milano, Edificio 6, Piazza Leonardo da Vinci 32, 20133 Milano, Italy. E-mail: roberto.piazza@polimi.it*
[c] *EMPA, Laboratory for Cellulose & Wood Materials, Überlandstrasse 129, 8600 Dübendorf, Switzerland*
[d] *ETH Zürich, Department of Materials, Wolfgang-Pauli-Strasse 10, 8093 Zürich, Switzerland*

2 Exploration of the parameters' space

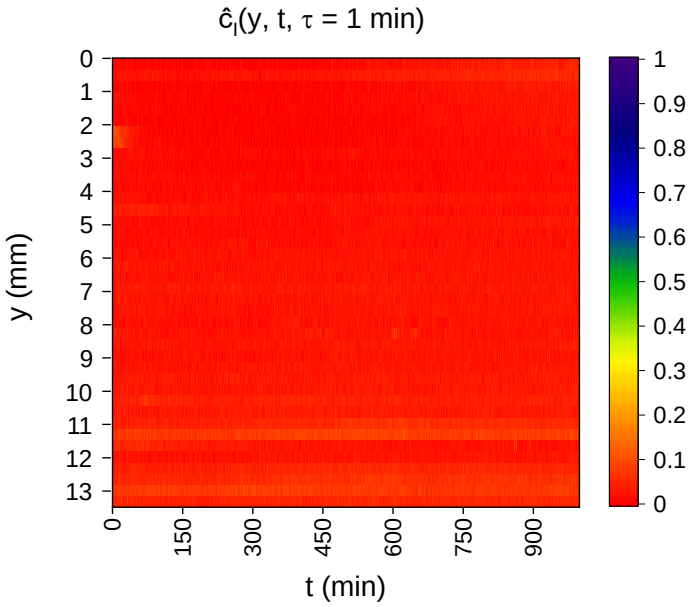

Fig. S2 Analysis of a 2 wt% βLG amyloid fibril sample in contact with a reservoir having an ionic strength of 100 mM, through computation of the space/time evolution of the correlation index. The methodology of the analysis is the same as the one employed in Fig.2 of the main text.

The phase diagram on the behaviour of βLG amyloid fibrils as a function of concentration and ionic strength was reported in previous publications[2,3]. More in detail, referring to the Supplementary Information of work of Cao et al., at our concentration of interest (2 wt%) the formation of transparent amyloid fibril gels can be promoted by ionic strengths that range between 60 and 125 mM. Considering the ratio between the volume of the added salt (1.5 mL) and the one of the amyloid fibril solutions (2 mL), these two equilibrium values are associated to initial ionic strengths in the reservoirs of $\sim$ 150 mM and $\sim$ 300 mM, respectively. Being the transparency of the sample an important pre-requisite for performing scattering experiments (to avoid undesired multiple-scattering phenomena), we considered 300 mM as the upper limit value for the ionic strength in the reservoir, and therefore did not explore values larger than such a limit. We explored ionic strengths in the range mentioned above (150 – 300 mM) and below 150 mM.

Fig.S2 represents the analysis of the space-time evolution of the correlation index, for a 2 wt% βLG amyloid fibril sample in contact with a reservoir having an ionic strength of 100 mM. Before analysis, the acquired images were corrected with the same procedure explained in section 4.1 of this document. As it is clearly visible, over the timescale of the performed experiment, the values of the correlation index do not suggest any gelation happening.

As a consequence of the considerations shared above, we decided to base our work on the two ionic strengths that lay at the boundaries of the interval we described, as they are the most diverse conditions that allow an optical characterisation (with negligible multiple scattering, that would be present at concentrations larger than 300 mM) without a separation between the ions' propagation and gelation timescales (that could occur at concentrations lower than 150 mM).

3 Rheological characterisation of the gels

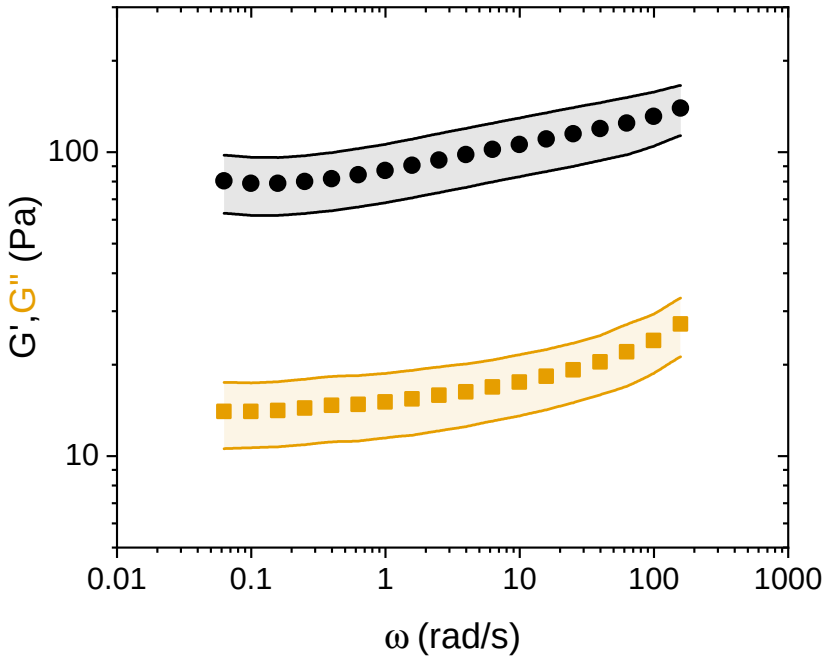

Fig. S3 Rheological characterization of the βLG amyloid fibril gels, through oscillatory sweeps performed at 1% strain with a plate-plate geometry. The samples were prepared as stated in the Materials and Methods section of the main text: more in detail, the shown curves are relative to gels prepared with a 300 mM NaCl solution. It can be appreciated how G' is one order of magnitude larger than G'', confirming the elastic properties of the sample.

4 Appearance of collected images before and after correction

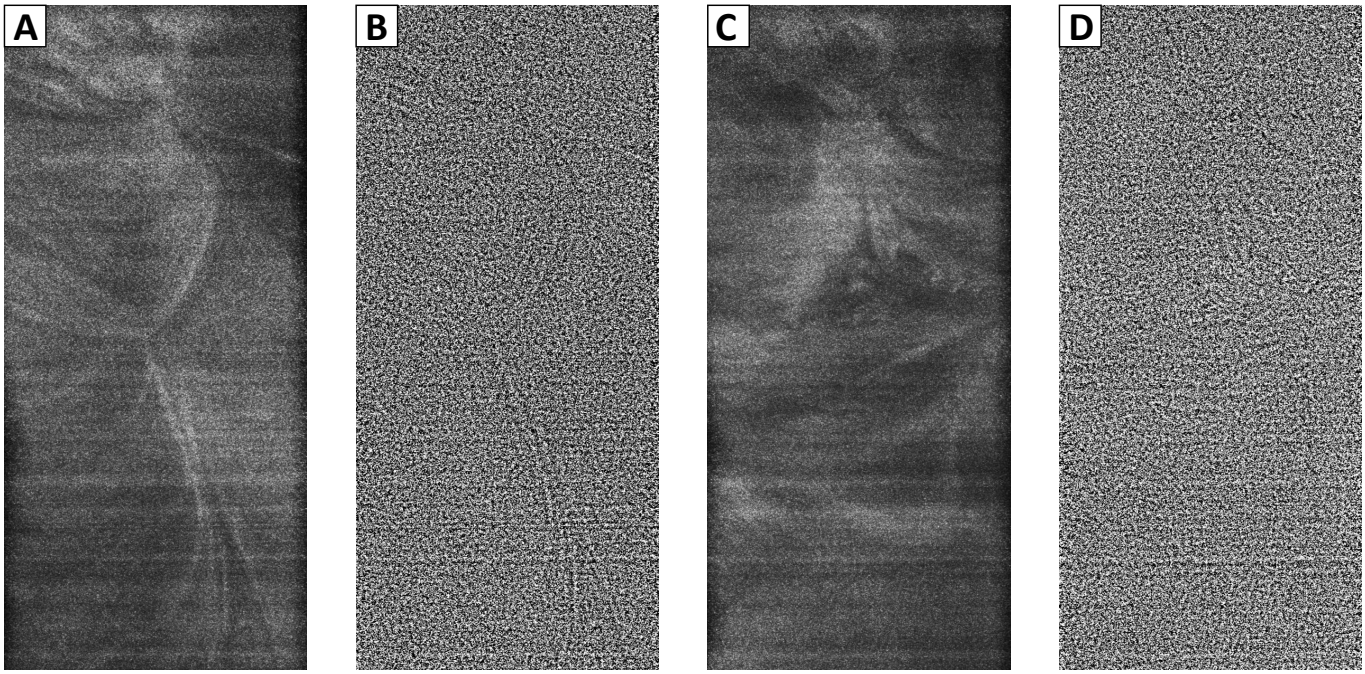

Fig. S4 Images acquired with the PCI (photon correlation imaging) setup. (**A**) Image acquired 500 min after the beginning of the 300 mM NaCl experiment. The noise has been previously subtracted. (**B**) Same image as in panel A, after correction for the uneven background. (**C**) Image acquired 500 min after the beginning of the 150 mM NaCl experiment. The noise has been previously subtracted. (**D**) Same image as in panel C, after correction for the uneven background.

4.1 Procedure for correcting the uneven background

The noise of the CMOS camera was determined by averaging 1000 images (2048 (V) $\times$ 1000 (H) pixels) acquired in dark conditions; such noise was subtracted to the raw images.

To minimize the influence of potentially in-homogeneous lighting of different zones of the cuvette and of background changes over time, an Average filter with radius 16 pixels (in the software ImageJ) was applied to each noise-corrected image; afterwards, the original noise-corrected image was divided by the result of the operation (with the final result being saved as a 32-bit output). The speckle field generated by the scattered light was still visible in the new set of images, as the characteristic size of light speckles ($\sim$ 2 pixels) was one order of magnitude smaller than the radius of the applied filter (16 pixels). Before being divided in ROIs, the obtained sets of images were cropped to final dimensions of 2000 (V) x 900 (H) pixels, to exclude areas that were external with respect to the cuvettes.

5 Decorrelation time-scales of amyloid fibril solutions and gels

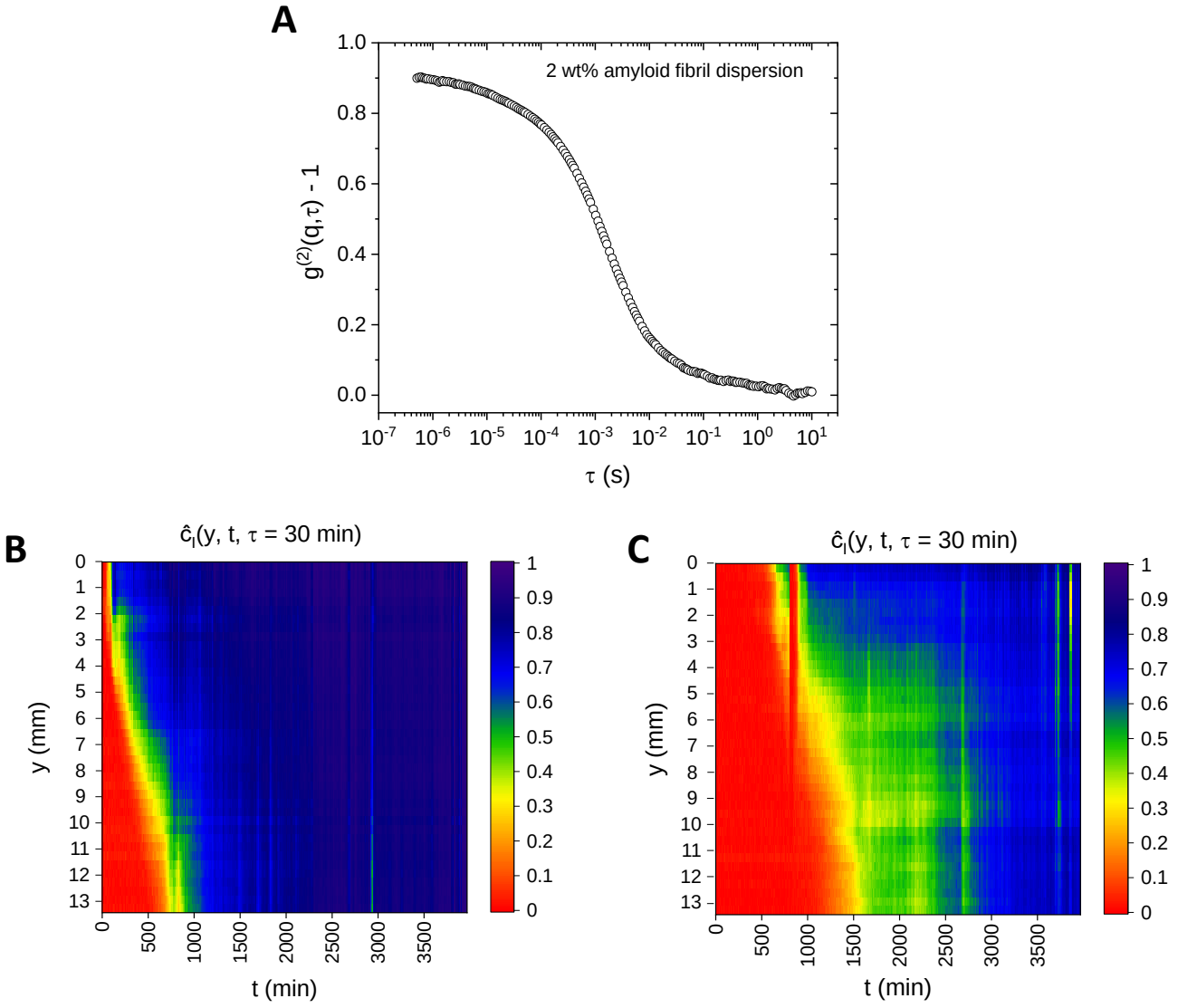

Fig. S5 (A) Dynamic light scattering (DLS) characterisation of an amyloid fibril dispersion at 2 wt%. (B,C) Computation of the space/time evolution of the correlation index (for HSM and LSM, respectively), considering a delay time $\tau = 30$ min. The methodology of the analysis is the same as the one employed in Fig.2 of the main text.

In the main text, the characteristic decorrelation time of amyloid fibril solutions and gels were reported ($10^{-4} - 10^{-2}$ s and $10^{1} - 10^{3}$ s, respectively). These two time ranges are extracted from auxiliary measurements we report below. Fig. S5(A) shows a dynamic light scattering characterisation of a 2 wt% amyloid fibril suspension, performed with a He-Ne laser ($\lambda = 632.8$ nm) at a measurement angle of 90°; the resulting probed q-vector (and the associated length-scale) are comparable to the ones of the PCI characterisation, as only the wavelength of the laser slightly changes ($\lambda = 632.8$ nm for the DLS characterisation and $\lambda = 532$ nm for the PCI ones, respectively). The collected intensity correlation function clearly shows a full decay within a time-scale of 10 s, and therefore suggests that the delay time used for the PCI characterisation ($\tau = 1$ min) is larger than characteristic time-scale associated to the dynamics of suspensions of amyloid fibrils. To show that $\tau = 1$ min is shorter that the characteristic relaxation time of the formed amyloid gels, we performed a further PCI characterisation at $\tau = 30$ min for both HSM and LSM samples (Fig.S5(B) and S5(C), respectively). Despite the larger delay time, the areas where a gel already formed stays highly correlated (when no temporally heterogeneous re-configurations occur). We infer therefore that the relaxation time of the gels (we mean the ones that are related to its

dynamics, and not to temporally intermittent events) is larger than 1 min.

6 Appearance of a formed amyloid fibril gel

Fig. S6 Picture of the transparency of a βLG amyloid fibril gel prepared through perfusion of ions from a 300 mM NaCl solution at pH 2. The well-known mathematical equation, behind the cuvette, can be clearly seen and read. The picture was taken eight days after the preparation of the system, to show the negligible role of shrinkage in βLG amyloid fibril gels.

7 Temporal evolution of the scattered intensity and of the correlation index

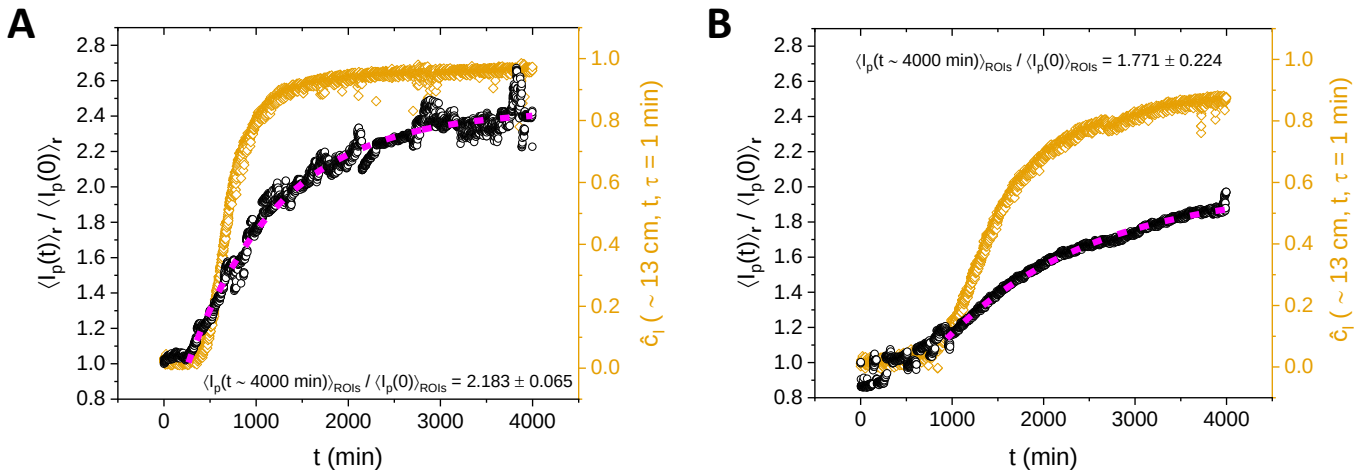

Fig. S7 Evolution of the average intensity in a ROI (50 V x 900 H) located at the bottom part of the cuvette (black circles), normalized to the average intensity at the beginning of the experiment, for the HSM (A) and LSM (B) samples. The curves are fitted (magenta dashed lines) with an exponential function ($\langle I_p(t)\rangle_\mathbf{r}/\langle I_p(0)\rangle_\mathbf{r} = I_0 + A(1-e^{(t-t_0)/\tau})$). In the two panels, the ochre diamonds represent the evolution of the correlation index $\hat{c}_I$ over time for the same ROIs. Moreover, each panel reports the value (mean $\pm$ standard deviation) of the final (t $\sim$ 4000 min) increase of the scattered intensity, averaged over multiple ROIs to take into account potential heterogeneities associated to different background contributions: this point is further discussed in section 7 of this document.

Important hints on the evolution of the gelation process can be obtained by the time evolution of the scattered intensity. For doing so, we first divided the images in ROIs having a lateral extension of 900 pixels (full width of the images) and a height of 50 pixels. Then, for each ROI, we computed the ratio between its average intensity at time t ($\langle I_p(t)\rangle_\mathbf{r}$) and its average intensity at $t = 0$ ($\langle I_p(0)\rangle_\mathbf{r}$), over the time-scale of the entire experiment ($t \sim 4000$ min). With I_p, we mean the local pixel intensity after noise subtraction; therefore, the correction for the uneven background (as illustrated in section 4.1 of the SI) was not applied to the images; in fact, as a consequence of the procedure, the information on the increase of scattered intensity would have been lost.

Fig. S7 shows the evolution of $\langle I_p(t)\rangle_\mathbf{r}/\langle I_p(0)\rangle_\mathbf{r}$ for ROIs located in the bottom part (y $\sim$ 13 cm) of the HSM and LSM cuvettes, respectively in panels A and B (black circles). While in HSM the intensity ratio increases of a factor $\sim$ 2.4, for LSM an increase of $\sim$ 1.8 is observed. Moreover, by comparing the evolution of the intensities with the one of the correlation indexes (ochre diamons), it is possible to appreciate differences between HSM and LSM. In the first case, the increase in correlation index happens on a time-scale that is faster than the one of the increase in scattered intensity: this suggests that, while gelation happens rather fast, further agglomeration phenomena (and therefore enhanced scattering) continue to happen in time. In the second case (LSM), the two mentioned time-scales are closer to each other, and therefore morphological changes happen in the same time-scale over which the gelation proceeds.

Regarding the increase in scattered intensity, further considerations are worth sharing. Being only the noise subtracted to the images, on top of the scattering pattern there are static background contributions, that are associated to potential local density in-homogeneity of the measured samples and to potential imperfections in the setup (e.g., properties of the illuminating laser sheet). To minimize the influence of such contributions in our analysis, on the side of reporting in panels A and B the time behaviour for a specific ROIs, we averaged the final values of increase in scattering intensity at different ROIs, which have different background contributions. We performed this analysis for the bottom half of the HSM images (N=19 ROIs) and for the full LSM images (N=40 ROIs): the decision of considering less than half of the HSM ROIs was caused by the fact that, in the beginning of the measurement, the upper part of the cuvette already experienced gelation and the increase in scattered intensity would have consequently been underestimated. The average values and the associated standard deviations ($\langle I_p(t \sim 4000 min)\rangle_{\mathbf{ROIs}}/\langle I_p(0)\rangle_{\mathbf{ROIs}}$) are reported as written text in the two panels: the average values close to 2 and the small associated standard deviations suggest that the performed analysis is robust and is not much influenced by local different backgrounds in different ROIs.

8 Beginning of the observations and physical phenomena in the proximity of the membrane

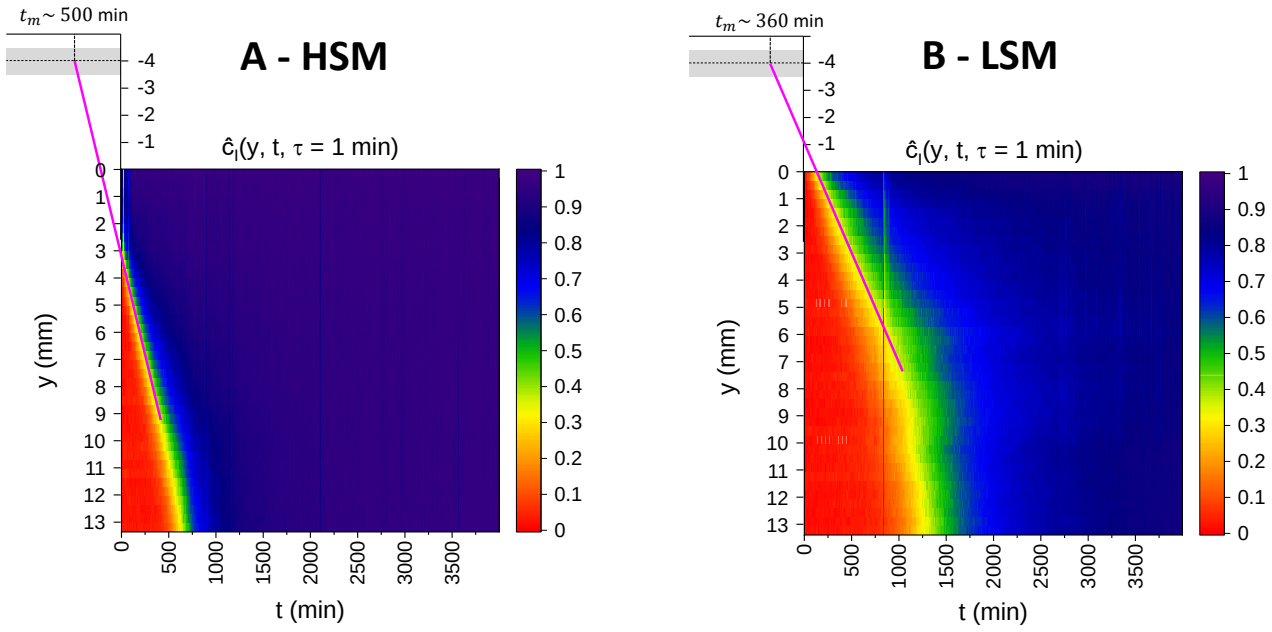

Fig. S8 Extrapolation of the observed linear behavior of the gelation front towards negative time values (in panels A and B for HSM and LSM, respectively), to shed light onto the physical phenomena that occur in the proximity of the membrane. The membrane is assumed to be at y = - 4 mm, with an error bar (grey area) of 0.5 mm.

8.1 Preparation of the samples and beginning of the observation

As mentioned in the main manuscript, the time 0 for both measurements corresponds to the beginning of the observations. When looking at panels A and B of Fig.2 in the main manuscript, some differences emerge. While for HSM, at t = 0 min, the upper 3 cm of the imaged area are already in a gel state (dark blue colour), for LSM it takes around 200 min for the first ROI to show hints of gelation. This difference can be explained considering that, for the two cases, the delays between the preparation of the sample and the beginning of the observation differ. In the case of HSM, the observation started more than 90 minutes after the preparation of the sample, as over the mentioned time span a further characterization was carried out (data not shown). In the case of LSM, the measurement started instead within 20 min from the preparation of the sample.

8.2 Physical phenomena in the proximity of the membrane

The different delays from the preparation of the samples to the beginning of the observations are, however, not sufficient to fully describe the physical phenomena that happen in the proximity of the membranes. On the basis of the observed linear advance of the gelation front, it is possible extrapolate the behaviour of the probed systems at times that lie outside the observation window. For both HSM and LSM, we used the extracted velocities of the evolving front (1.47×10^{-2} mm/min and 7.77×10^{-3} mm/min, respectively), together with the assumed position of the dialysis membrane ($\sim$ - 4 mm for both cases), to check whether an extrapolation towards negative time values allows to obtain delay times, that are compatible with the ones reported above (90 and 20 min for HSM and LSM, respectively). The obtained results are reported in Fig.S8 ($\sim$ 500 min and $\sim$ 360 min for HSM and LSM, respectively) and hardly agree with the reported delays: in the following, we share hypotheses that might explain this mismatch.

Firsly, we hypothesize that the reported value of the position of the membrane is inaccurate. It might be that inaccuracies, in cutting and in positioning the syringe inside the cuvette, introduce complications in determining the exact position of the dialysis membrane. If the membrane was nearer to the observation area than the reported value (- 4 mm), the results of the extrapolation would get closer to the reported delay times. However, this first hypothesis is not sufficient to fully

explain the observed difference.
As second hypothesis, we assume that the linear behaviour observed in the probed area is not valid in the proximity of the membrane. A first fact that supports this hypothesis is that, after adding salt to the syringes, the studied systems were sealed with parafilm. It might be that this manual operation induced a shaking that speed-ed up the salt perfusion at an initial stage. A second point that aligns with this hypothesis is the difference between the liquid height within and outside from the syringe. Despite the syringe was partially immersed in the amyloid fibrils solution, to ensure contact between the colloidal dispersion and the dialysis membrane, the level of the liquid inside the syringe was higher than the the one of the liquid between the syringe and the cuvette (despite a modest increase related to the mentioned immersion). As a consequence, the arising hydrodynamic unbalance could favour the passage of a modest quantity of salt solution, that further speeded up the gelation phenomena in the proximity of the membrane. A more detailed analysis of this hypothesis is inhibited from the fact that the system, being sealed with parafilm, is not in contact with atmospheric pressure; therefore, a passage of liquid from the syringe to the cuvette would decrease the pressure inside the syringe while increasing the one in the cuvette.
The combination of the shared hypotheses allows to qualitatively describe the mismatch between the reported delay times and the computed extrapolation. A deeper analysis of this point goes beyond the scope of this work: in fact, the decision of sampling an area with a few mm distance from the membrane was done appositely to avoid dealing with hard-to-describe physical phenomena in its proximity, among which we also account the change in cross-section (from circular to quadratic) between the syringe and the cuvette.

9 Stress releasing events during the advance of the gelation front

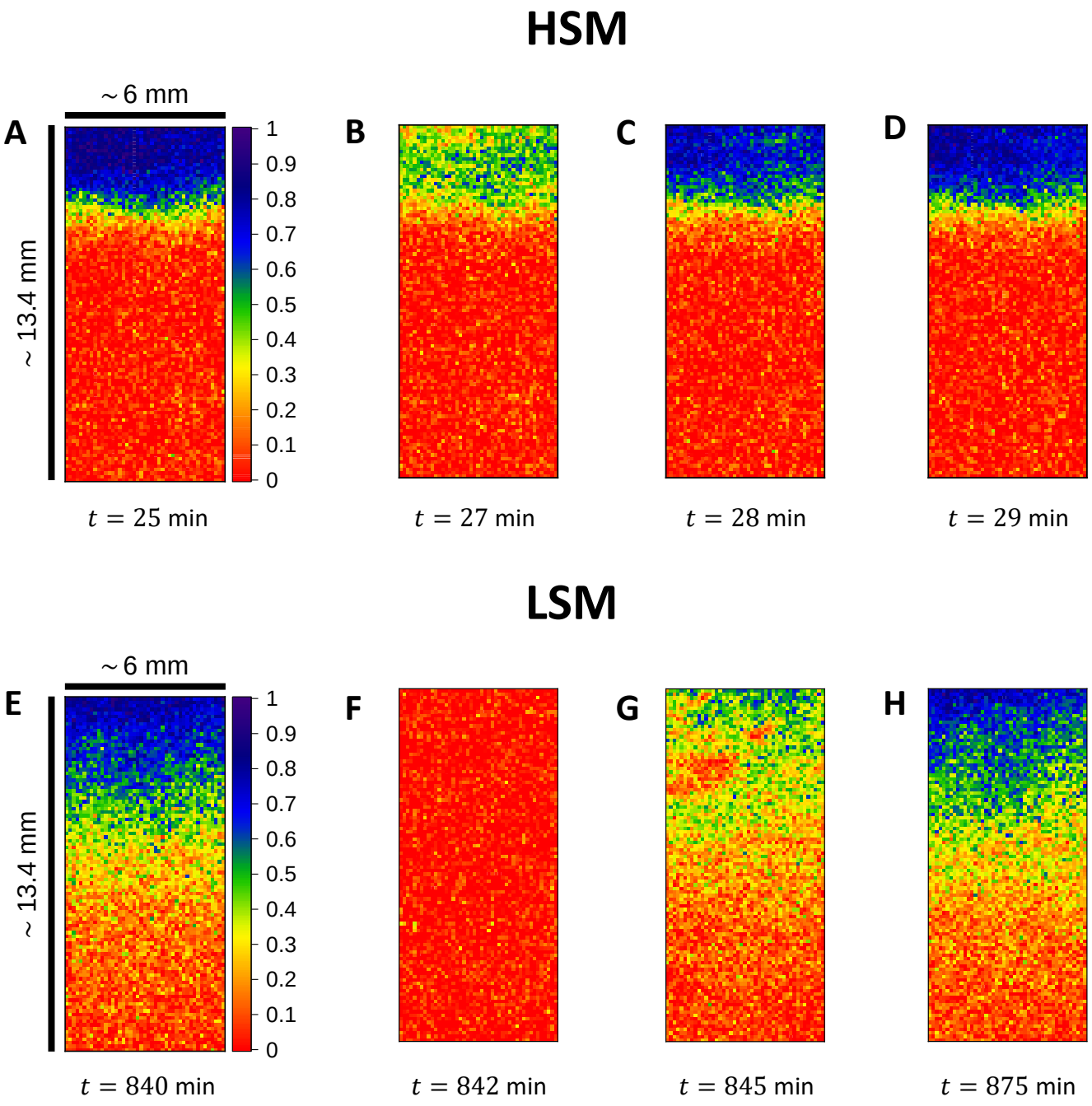

Fig. S9 Stress-releasing events that happened while the gel was forming in the probed area, shown through DAMs computed at a constant delay time (τ) of 1 min. (A-D) Modest and fast-recovering decorrelation burst in HSM. (E-H) Significative and slow-recovering decorrelation burst in LSM.

In the main text, we discussed stress-releasing events that happened after the gel had formed in the entire probed area, for both HSM and LSM. Here we show (Fig.S9) that stress-releasing events also accompanied the creation of an arrested phase. In panels A-D, a decorrelation burst that characterizes HSM gelation is reported. At 25 minutes (A), a gel layer is formed in the upper part of the cuvette, while the middle and bottom parts shows a fully decorrelated state. Two minutes later (B) the correlation index drops where the gel had already formed: despite very limited hints of total correlation, the area shows a green-like colour that is associated to $\hat{c}_I$ values close to 0.5. One and two minutes later (C and D,

respectively), the upper part of the cuvette shows again high correlation values.
A similar (but more drastic) phenomenon happened in LSM (E-H). At 840 minutes from the beginning of the observation, the upper part of the cuvette showed the formation of a gel layer (E). Two minutes later (F) all the ROIs in the DAM gets fully uncorrelated (F): this is related to a major stress-release event that allows the network to reconfigure itself, in a configuration which is energetically more stable. Later on, the system slowly re-gains higher correlation values in the zone where the gel already formed (G-H).
When comparing the magnitude of the two decorrelation burst and the recovery time after them, key differences emerge between HSM and LSM. While in LSM the correlation index drops everywhere to close-to-0 values, in HSM hints of local correlation remain. Even more remarkably, while in HSM close-to-1 values of the correlation index are regained within 1 minutes, LSM needs many more minutes to find and fix a new configuration. In fact, the lower concentration of salt reduces the probability of transforming entanglements into physical cross-links, with consequent larger susceptibility of the network to further motion of the forming units.

References

[S1] I. Usov and R. Mezzenga, *Macromolecules*, 2015, **48**, 1269–1280.

[S2] S. Bolisetty, L. Harnau, J.-m. Jung and R. Mezzenga, *Biomacromolecules*, 2012, **13**, 3241–3252.

[S3] Y. Cao, S. Bolisetty, J. Adamcik and R. Mezzenga, *Physical Review Letters*, 2018, **120**, 158103.